Research Article

Polarization properties of few-layer graphene on silicon substrate in terahertz frequency range

Anatoly Kvitsinskiy[1,2] · Petr Demchenko[1,2] · Alexander Grebenchukov[1,2] · Egor Litvinov[1,2] · Maxim Masyukov[1] · Anton Zaitsev[1,2] · Anna Baldycheva[3] · Evgeniya Kovalska[3] · Anna Vozianova[1] · Mikhail Khodzitsky[1,2]

Received: 5 August 2019 / Accepted: 21 November 2019 / Published online: 28 November 2019

Abstract
Terahertz time-domain spectroscopic polarimetry (THz-TDSP) method was used to study polarization properties of a few-layer graphene (FLG) on a silicon (Si) substrate in terahertz (THz) frequency range under an external optical pumping and an external static magnetic field. Frequency dependencies of azimuth and ellipticity angles of a polarization ellipse and the polarization ellipse at various frequencies of the electromagnetic waves transmitted through the Si substrate and the FLG on the Si substrate were obtained experimentally and theoretically. The results confirm the fact that, based on the FLG, it is possible to devise efficient tunable THz polarization modulators for use in the latest security and telecommunication systems.

Keywords Terahertz time-domain spectroscopic polarimetry · Few-layer graphene · High-resistivity monocrystalline silicon · Polarization properties · Stokes parameters · Faraday effect

PACS Nos. 07.57.Pt · 42.25.Ja · 42.79.Ci · 68.65.Pq · 75.70.Cn · 78.20.Ls

1 Introduction

Terahertz (THz) radiation is widely used in physics and astronomy [1–3], chemistry and medicine [4–6], security and telecommunication systems [7–9], and other fields of science and technology [10].

Currently, one of the relevant problems for development of THz photonics is the lack of efficient and affordable tunable under external influences devices for modulating the polarization of an electromagnetic radiation in the THz frequency range [11–15]. Polarization, amplitude, and frequency modulators are basic components in the security and telecommunication systems, for example, for communication between geostationary satellites. The efficient polarization modulators have a fundamental importance for an investigation of properties of novel materials in physics and chemistry.

A promising solution to the foregoing problem is a study of graphene for use as a functional medium in polarizers thanks to unique optical and electronic properties of this material. From a point of view of physics, one of the ways to control polarization properties of graphene is to use the magneto-optical Faraday effect.

In this regard, recent research is concentrated in a field of studying an influence of an external optical pumping (OP), and an external static magnetic field (MF) on the properties of graphene, especially of few-layer graphene (FLG), which generally contains from 3 to 10 layers.

✉ Anatoly Kvitsinskiy, anatolykvitsinskiy@gmail.com; Mikhail Khodzitsky, khodzitskiy@yandex.ru | [1]Terahertz Biomedicine Laboratory, ITMO University, 3b Kadetskaya Liniya, Saint Petersburg, Russian Federation 199034. [2]Center for Bioengineering, ITMO University, 49 Kronverksky Prospekt, Saint Petersburg, Russian Federation 197101. [3]Graphene Centre, University of Exeter, Stocker Road, Exeter EX4 4QL, UK.

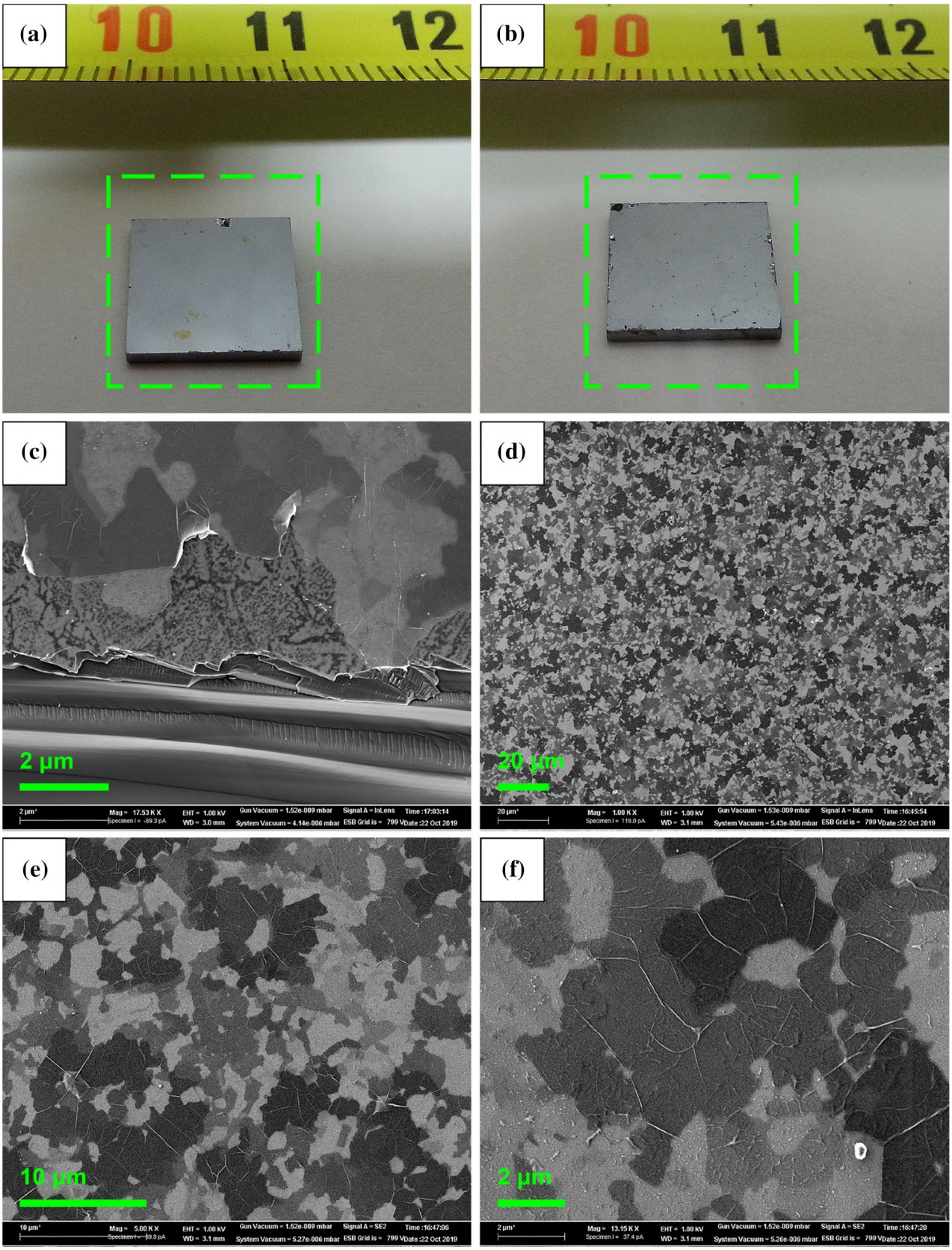
(a)
10
11
12
(b)
10
11
12
(c)
2 µm
(d)
20 µm
(e)
10 µm
(f)
2 µm

◂**Fig. 1** Pictures of **a** the Si substrate, and **b** the FLG on the Si substrate, highlighted in green, with the scale bar of 2 cm; **c** SEM image of the side view of the FLG on the Si substrate with the scale bar of 2 μm; and SEM images of the top view of the FLG on the Si substrate with the scale bars of **d** 20 μm, **e** 10 μm, and **f** 2 μm

Firstly, it is worth noting several works devoted to the study of properties of the graphene under the OP. An article by Gu et al. [16] is devoted to a theoretical research of a FLG on a lithium niobate substrate, with the number of graphene layers from 2 to 8, in the frequency range from 0.5 to 10 THz. It has been shown that the transmittance and the reflectance of the FLG can be adjusted by changing the number of the layers and the intensity of the OP. Ryzhii et al. [17] theoretically studied a bilayer graphene (BLG), in the frequency range from 1 to 10 THz. It has been shown that the remote doping enhances the indirect interband generation of photons in the BLG. Fu et al. [18] experimentally studied a vertically aligned FLG on a quartz substrate, with the number of graphene layers from 5 to 10, in the frequency range from 0.1 to 1.5 THz. It has been shown that the optical conductivity of the photoexcited vertically aligned FLG has a strong free carrier response. Fu et al. [19] experimentally studied a single-layer graphene (SLG) on a quartz substrate, in the frequency range from 0.1 to 1.5 THz. It has been shown that the transmission of the SLG increases nonlinearly with the increase in the intensity of the OP. Tomadin et al. [20] theoretically and experimentally studied the ultrafast carrier dynamics and the photoconductivity of a SLG on a quartz substrate.

Secondly, there are several interesting works devoted to the study of properties of the graphene under the MF. An article by Heyman et al. [21] is devoted to an experimental research of a SLG in a sapphire substrate. In this paper, data on the conductivity and the carrier scattering rate of the SLG are described in detail. Qin et al. [22] theoretically studied the rate of the Faraday rotation of a SLG with a gold grating on a silicon (Si) substrate, in the frequency range from 0.43 to 24 THz. Liu et al. [23] theoretically studied multilayered graphene disks on a substrate, with the number of graphene layers from 2 to 5, in the frequency range from 15 to 45 THz. It has been shown that the Faraday rotation is due to the plasmonic coupling in the graphene disks. Mei et al. [24] theoretically and experimentally studied the magneto-optical properties of a BLG and a trilayer graphene (TLG) on quartz substrates, in the frequency range from 0.1 to 2.0 THz. Grebenchukov et al. [25] theoretically studied the magneto-optical properties of a multilayer graphene (MLG) on a dielectric substrate, at the frequency of 1.0 THz.

Summarizing, it could be concluded that studies of the optical properties of FLG and MLG depending on the number of the layers and the substrate material under the external influences in the THz frequency range, however, are principally theoretical, or limited to three layers of graphene.

To experimentally obtain the necessary polarization and magneto-optical properties of carbon nanomaterials and nanostructures, the THz time-domain spectroscopic polarimetry (THz-TDSP) method is widely used [26–30].

Therefore, the objective of this work was a study of a FLG on a Si substrate using the THz-TDSP method to obtain its polarization properties and to devise tunable THz polarizers based on it.

In this work, polarization properties of the FLG on the Si substrate under the OP and the static MF were obtained experimentally and theoretically in the frequency range from 0.2 to 1.0 THz.

It was found that with the simultaneous use of the OP and the static MF, the azimuth angle of a polarization ellipse changes on average by 6°. This is enough to devise compact magneto-optically tunable polarizers based on the FLG, which are necessary in advanced THz nanophotonics.

2 Material and methods

The FLG on the Si substrate and the sample of the Si substrate were studied. The FLG was synthesized by the chemical vapor deposition at University of Exeter's Graphene Centre (UK) [31]. The FLG was grown on a nickel (Ni) foil in a quartz chamber using argon, hydrogen, and methane gases. The Ni foil with a thickness of 25.0 μm was used as a catalyst for the growth of the FLG. The Ni foil was etched in an iron(III) chloride hexahydrate solution, and then, the FLG was transferred to the Si substrate with a surface area of ~ 1.0 cm^2 and a thickness of ~ 1.0 mm. The high-resistivity monocrystalline Si substrate was grown at Tydex (Russian Federation).

To study a surface morphology of the FLG on the Si substrate, scanning electron microscopy (SEM) images were obtained at various scales. Pictures of the Si substrate, the FLG on the Si substrate, and SEM images of the FLG on the Si substrate are shown in Fig. 1. Based on the SEM images, it can be seen that the graphene is distributed over the surface of the Si substrate in the form of disordered flakes with a diameter of ~ 10 μm, with a different brightness, which also means a different number of layers.

To determine the number of the layers of the experimental sample, reflection Raman spectroscopy was performed. Raman spectra of the FLG on the Si substrate are shown in Fig. 2. Raman spectra were recorded for one of the light and one of the dark graphene flakes using 514.5 nm laser excitation system [32], 50× objective, and 10 s integration time for a single scan. By studying the

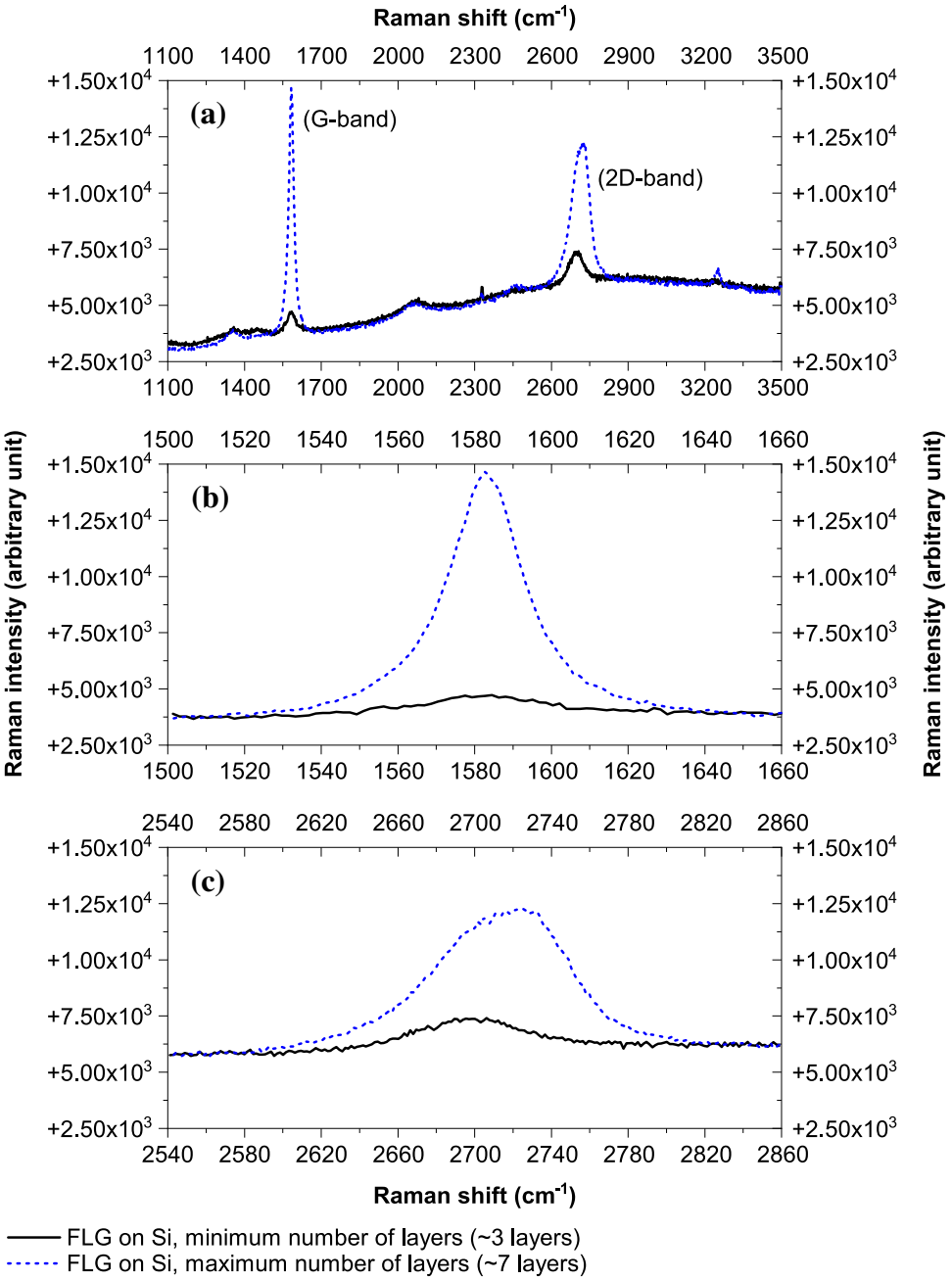

Fig. 2 Raman spectra of the FLG on the Si substrate **a** in the full scale, and the scaled parts containing **b** the G-bands, and **c** the 2D bands of the spectra

spectra and intensity of main characteristic peaks of MLG (the G-bands at ~ 1580 cm^{-1} and the 2D bands at ~ 2700 cm^{-1}), it was found that the experimental sample contains a minimum of ~ 3 and a maximum of ~ 7 layers of graphene [33].

To study the polarization properties of the experimental samples using the THz-TDSP method, a system based on a THz time-domain spectrometer [34], two polarizers, a 980 nm laser for creating the OP of ~ 1.0 W · cm^{-2}, and a NdFeB axially magnetized magnet for creating the static MF of ~ 1.3 T was used.

A scheme of an experimental setup, schematic representation of the FLG on the Si substrate under the various external influences, pictures of an assembled experimental THz-TDSP setup, and a cuvette for the experimental samples are shown in Fig. 3.

A beam of a femtosecond Yb:KYW 1040 nm laser (LSR1) is divided by a beam splitter into a pump beam and a probe beam with 90% and 10% intensity. The pump beam goes through an optical delay line (ODL) and an optical chopper (OC) and falls on a InAs crystal (TS). The Dember effect occurs in this crystal. Because the mobility of

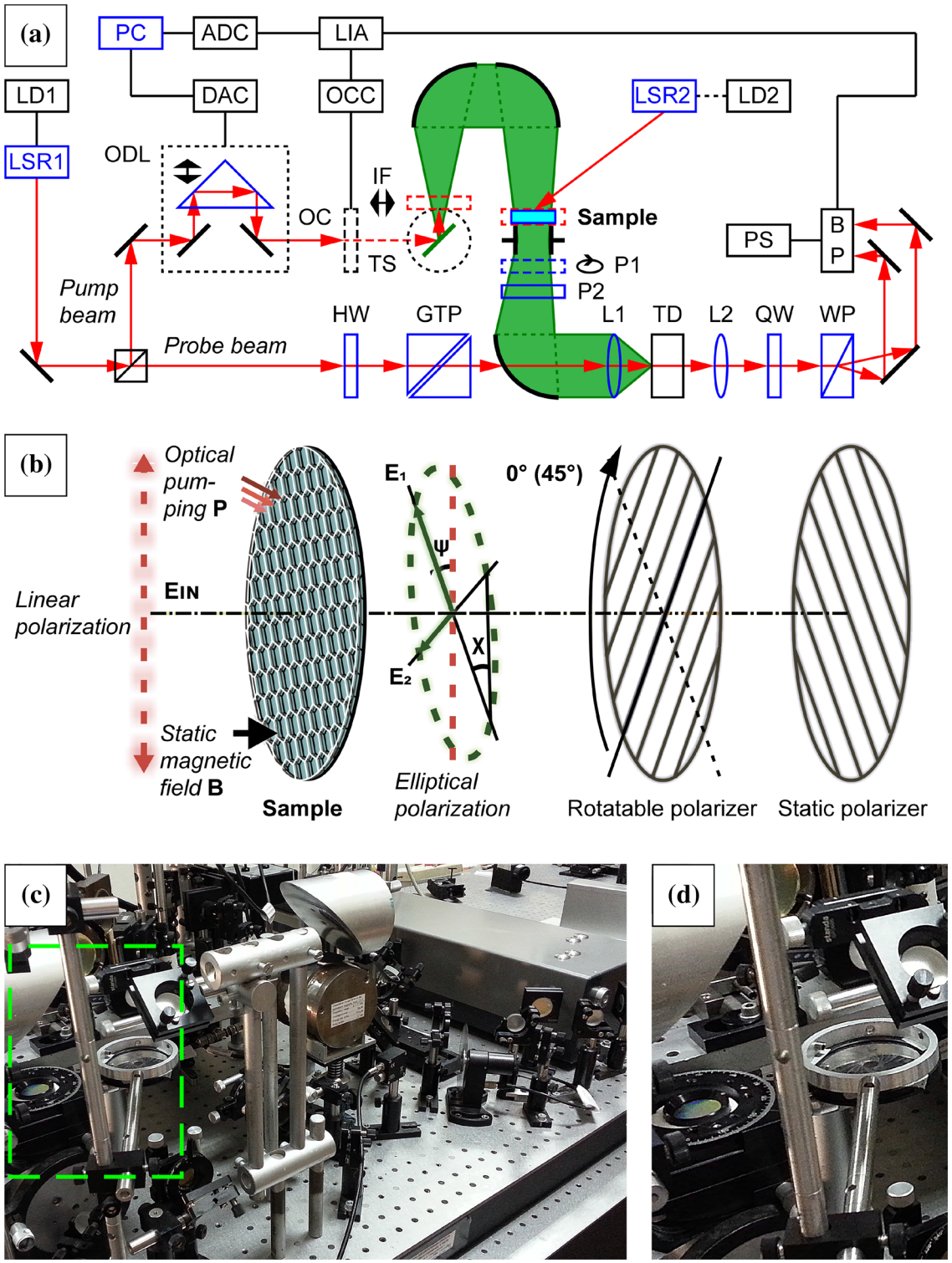

Fig. 3 **a** Scheme of the experimental THz-TDSP setup (ADC—analog-to-digital converter; BP—balanced photodetector; DAC—digital-to-analog converter; GTP—Glan–Taylor prism; HW—half-wave plate; IF—polytetrafluoroethylene (PTFE) infrared cut-off filter; L1, L2—positive lenses; LD1, LD2—laser diodes' drivers; LIA—lock-in amplifier; LSR1—femtosecond Yb:KYW 1040 nm laser; LSR2—980 nm laser; OC—optical chopper; OCC—optical chopper controller; ODL—optical delay line; P1—rotatable polarizer; P2—static polarizer; PC—personal computer; PS—balanced detector power supply; QW—quarter-wave plate; TD—THz radiation detector based on the CdTe crystal; TS—THz radiation source based on the InAs crystal; WP—Wollaston prism); **b** schematic representation of the FLG on the Si substrate under the various external influences; and pictures of **c** the assembled experimental THz-TDSP setup, and **d** the cuvette for the experimental samples

electrons is greater than the mobility of holes, electric dipoles are formed, which oscillate in the THz frequency range. The static MF of ~ 2.4 T is necessary to enhance an output THz radiation. The THz beam focuses on the experimental sample and then goes through two polarizers. The first polarizer (P1) is rotatable, and the second polarizer (P2) is static.

By recording temporal waveforms of transmitted THz signals at two different positions of the polarizers, it is possible to calculate the Stokes parameters and fully describe the polarization properties of the experimental samples.

The probe beam goes through a half-wave plate (HW) and a Glan–Taylor prism (GTP) and falls on a CdTe crystal (TD). The Pockels electro-optic effect occurs in this crystal. When the probe beam falls on the CdTe crystal simultaneously with the THz radiation, the CdTe crystal becomes anisotropic for the probe beam. The polarization of the probe beam becomes elliptical.

The probe beam goes through a quarter-wave plate (QW) and is divided by a Wollaston prism (WP) into two linearly polarized beams with orthogonal polarization. These beams are detected by a balanced photodetector (BP), and a received signal is transmitted to a personal computer (PC).

Temporal waveforms of the THz signals transmitted through the experimental samples under the various external influences were recorded using PC with LabVIEW® (National Instruments Corp., USA) software at the parallel and the crossed by 45° positions to a transmission direction of the polarizers. Each single measurement took ~ 35 min.

All measurements were taken at ITMO University's Terahertz Biomedicine Laboratory (Russian Federation) under a stable air temperature of ~ 291 K and a relative humidity of ~ 40%. Experimental temporal waveforms of the THz signals are shown in Figs. 4, 5 and 6.

Based on the waveforms, it can be seen that the electric field amplitude of the THz signals transmitted through the samples at crossed by 45° position to the transmission direction of the polarizers is approximately two times less than the corresponding amplitude at parallel positions in all cases.

It is also seen that when using the external OP, the amplitude also decreases by approximately half relative to the measurements without the OP in all cases. Since during the experiments, the surface of the samples was heated by ~ 20 K under the influence of the intensive infrared OP, the signal-to-noise ratio (SNR) decreased when recording waveforms.

Raw experimental data processing was done using MATLAB® (The MathWorks Inc., USA) software. To obtain the maximum SNR, denoising technique with Coiflet wavelet of order 4 and rectangular signal windowing were used. Compared to the other wavelets, such as Symlet, Daubechies, and Meyer, Coiflet denoising is the most optimal method for the THz signals processing [35]. The signal windowing was used to exclude an influence of a water vapor absorption.

3 Results

Experimental frequency dependencies of an azimuth angle ψ and an ellipticity angle χ of a polarization ellipse of the electromagnetic waves transmitted through the samples were calculated according to the formulas [36]:

$$\begin{bmatrix} S_0 \\ S_1 \\ S_2 \\ S_3 \end{bmatrix} = \begin{bmatrix} E_1^2 + E_2^2 \\ E_1^2 - E_2^2 \\ 2 \cdot E_1 \cdot E_2 \cdot \cos\delta \\ 2 \cdot E_1 \cdot E_2 \cdot \sin\delta \end{bmatrix}, \tag{1}$$

$$\begin{bmatrix} \psi_{\text{experiment}} \\ \chi_{\text{experiment}} \end{bmatrix} = \begin{bmatrix} 0.5 \cdot \tan^{-1}\left(S_2 \cdot S_1^{-1}\right) \\ 0.5 \cdot \sin^{-1}\left(S_3 \cdot S_0^{-1}\right) \end{bmatrix}, \tag{2}$$

where E_1 and E_2 are amplitudes of parallel and perpendicular components of an electric field vector $\boldsymbol{E}$, and δ is a phase difference between them. The results are shown in Fig. 7a, b, c, e, f, g. Polarization ellipse of the electromagnetic waves at the various frequencies transmitted through the samples is shown in Fig. 8.

4 Discussion

The conductivity of graphene in the static MF is described theoretically by a tensor with components [37]:

$$\begin{aligned} \sigma_{xx}(\omega) = \sigma_{yy}(\omega) &= \sigma_0 \cdot (1 - i \cdot \omega \cdot \tau) \\ &\times \left[(1 - i \cdot \omega \cdot \tau)^2 + \left(\omega_c \cdot \tau\right)^2\right]^{-1}, \\ \sigma_{xy}(\omega) = -\sigma_{yx}(\omega) &= \sigma_0 \cdot \omega_c \cdot \tau \\ &\times \left[(1 - i \cdot \omega \cdot \tau)^2 + \left(\omega_c \cdot \tau\right)^2\right]^{-1}, \end{aligned} \tag{3}$$

where $\omega_c = e \cdot B \cdot v_F \cdot \hbar^{-1} \cdot {k_F}^{-1}$ is an orbital cyclotron frequency; B is a magnetic field; $\sigma_0 = 2 \cdot e^2 \cdot \pi^{-1} \cdot \hbar^{-1}$ is a direct current conductivity; and $k_F = (4 \cdot \pi \cdot \Sigma)^{0.5}$ is a Fermi wave number, which depends on a carrier density $\Sigma = \Sigma_0 + \Delta\Sigma$, and can be controlled by OP.

Theoretical frequency dependencies of the azimuth angle ψ and the ellipticity angle χ of the polarization ellipse of the electromagnetic waves transmitted through the FLG were calculated according to the formulas [37]:

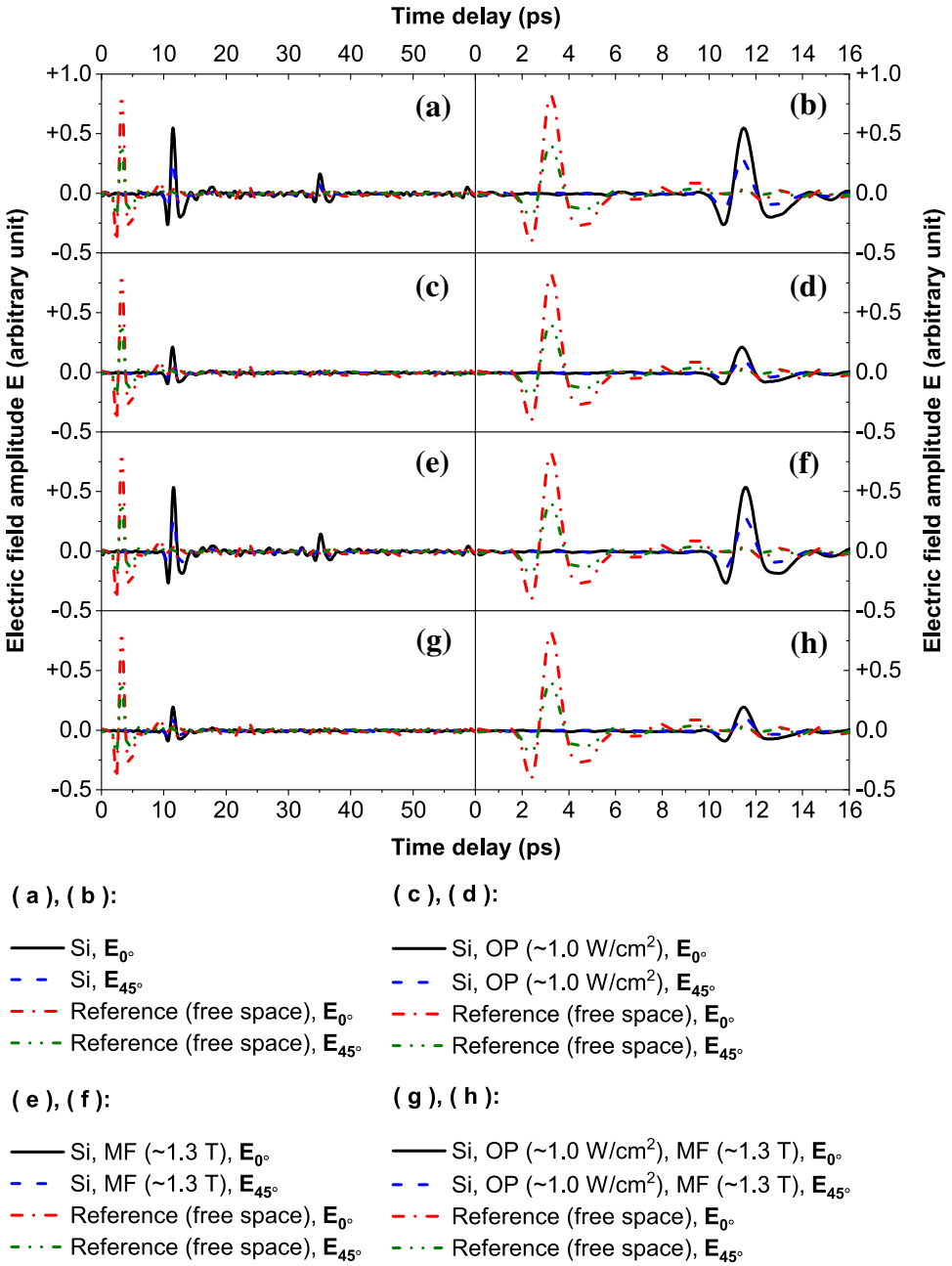

Fig. 4 Experimental temporal waveforms of the THz signals **a** in the full scale, and **b** the scaled part containing the main information of the signals transmitted through the Si substrate without the external influences; **c** in the full scale, and **d** the scaled part containing the main information of the signals transmitted through the Si substrate with the external OP; **e** in the full scale, and **f** the scaled part containing the main information of the signals transmitted through the Si substrate with the external static MF; **g** in the full scale, and **h** the scaled part containing the main information of the signals transmitted through the Si substrate with the external OP, and external static MF at parallel and crossed by 45° positions to the transmission direction of the polarizers

$$\begin{bmatrix}\psi_{\text{theory}}\\ \chi_{\text{theory}}\end{bmatrix} = \begin{bmatrix}0.5\cdot\tan^{-1}\left\{2\cdot\Re(\alpha)\cdot\left(1-|\alpha|^2\right)^{-1}\right\}\\ 0.5\cdot\sin^{-1}\left\{2\cdot\Im(\alpha)\cdot\left(1+|\alpha|^2\right)^{-1}\right\}\end{bmatrix}, \quad (4)$$
$$\alpha = 2\cdot\Sigma_{xy}\cdot\left(4+2\cdot\Sigma_{xx}\right)^{-1},$$

where $\Sigma_{xx}=\sigma_{xx}\cdot d\cdot Z_0$ and $\Sigma_{xy}=\sigma_{xy}\cdot d\cdot Z_0$ are effective dimensionless 2D conductivities; d is a film thickness; and Z_0 is the vacuum impedance.

Based on this theory, a mathematical model was developed [25] that describes polarization properties of the graphene depending on the number of layers and the external influences in the THz frequency range. The results are shown in Fig. 6d, h. This model is calculated on an assumption that the graphene consists of identical sheets stacked on top of one another, has no substrate, and is in vacuum. At the same time, the data shown in Fig. 6c, g were obtained by subtracting the data of the FLG on the Si substrate from the data of the Si substrate itself.

Figures 6 and 7 show that the most efficient method for controlling the polarization properties of the FLG is the

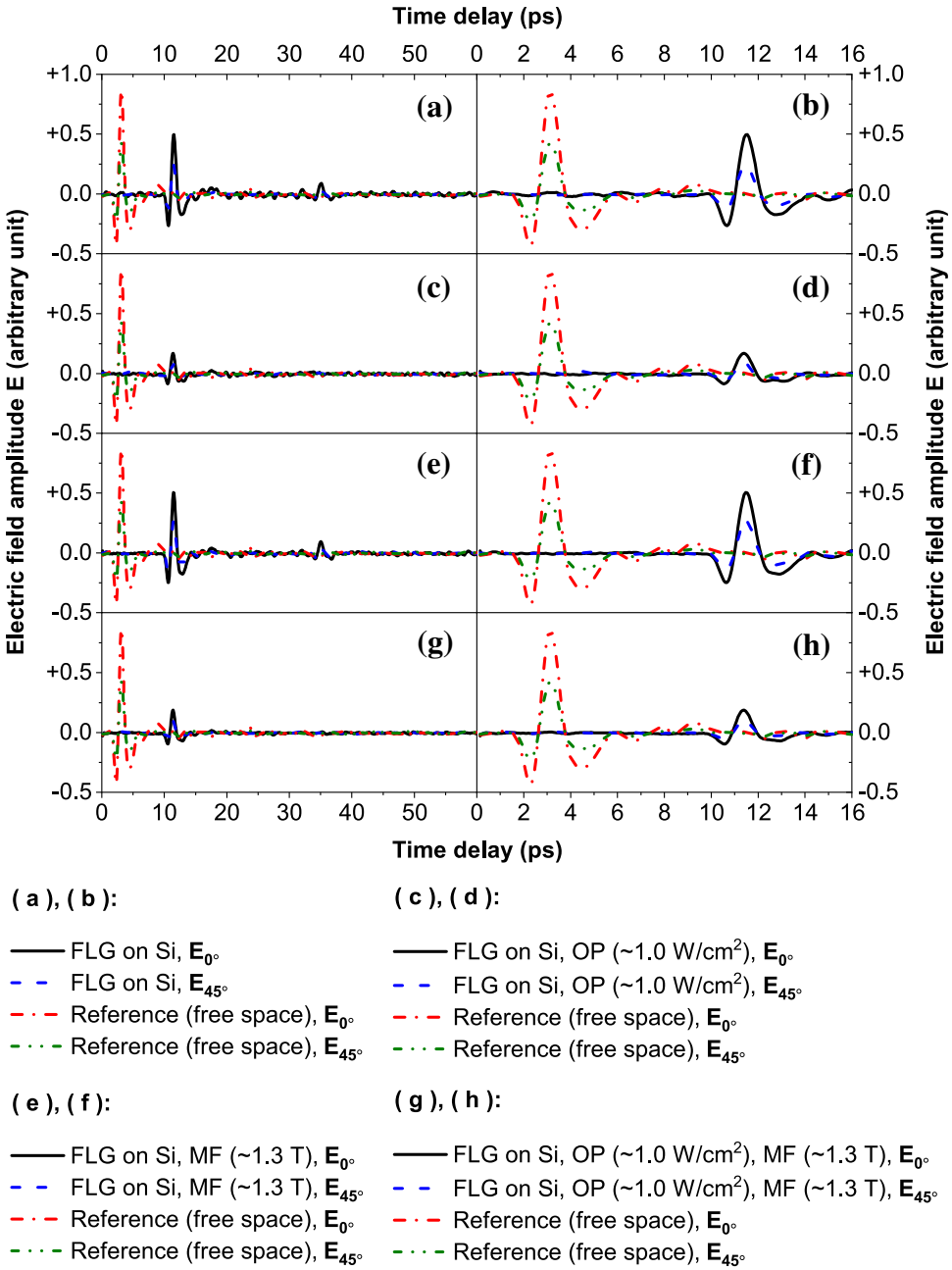

Fig. 5 Experimental temporal waveforms of the THz signals **a** in the full scale, and **b** the scaled part containing the main information of the signals transmitted through the FLG on the Si substrate without the external influences; **c** in the full scale, and **d** the scaled part containing the main information of the signals transmitted through the FLG on the Si substrate with the external OP; **e** in the full scale, and **f** the scaled part containing the main information of the signals transmitted through the FLG on the Si substrate with the external static MF; **g** in the full scale, and **h** the scaled part containing the main information of the signals transmitted through the FLG on the Si substrate with the external OP, and external static MF at parallel and crossed by 45° positions to the transmission direction of the polarizers

simultaneous use of the OP and the static MF. In this case, the azimuth angle changes on average by 6° relative to the FLG without influences, which is within the obtained theoretical data. Also, the ellipticity angle varies within 2°, which is noticeably less than the theoretical data. An effect of the Si substrate is also very noticeable, especially in the frequency range from 0.8 to 1.0 THz. This is confirmed by a form of the polarization ellipse.

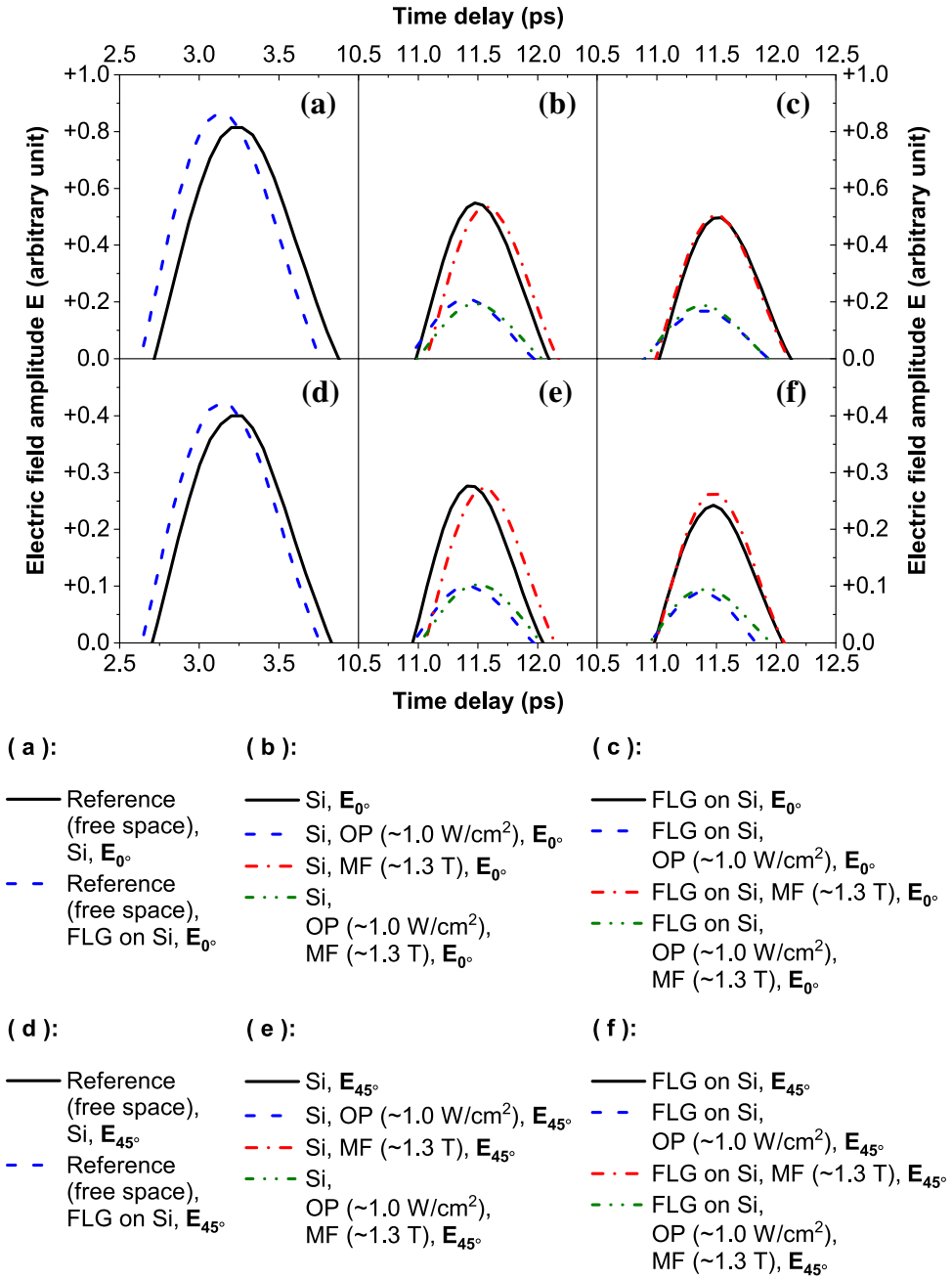

Fig. 6 Main peaks of the THz signals transmitted through **a** the reference (free space) for the Si substrate, and the FLG on the Si substrate; **b** the Si substrate; and **c** the FLG on the Si substrate under the various external influences at parallel positions to the transmission direction of the polarizers; and main peaks of the THz signals transmitted through **d** the reference (free space) for the Si substrate, and the FLG on the Si substrate; **e** the Si substrate; and **f** the FLG on the Si substrate under the various external influences at crossed by 45° positions to the transmission direction of the polarizers

The changes in the angles are a result of the magneto-optical Faraday effect. The difference between the theoretical and the experimental data is due to a simplicity of the mathematical model, which does not consider the effect of the Si substrate on the polarization properties of the graphene. Also, the complex morphology of the surface of the FLG, consisting of graphene flakes, which was confirmed by the SEM images, has an effect on the modulation of the polarization properties.

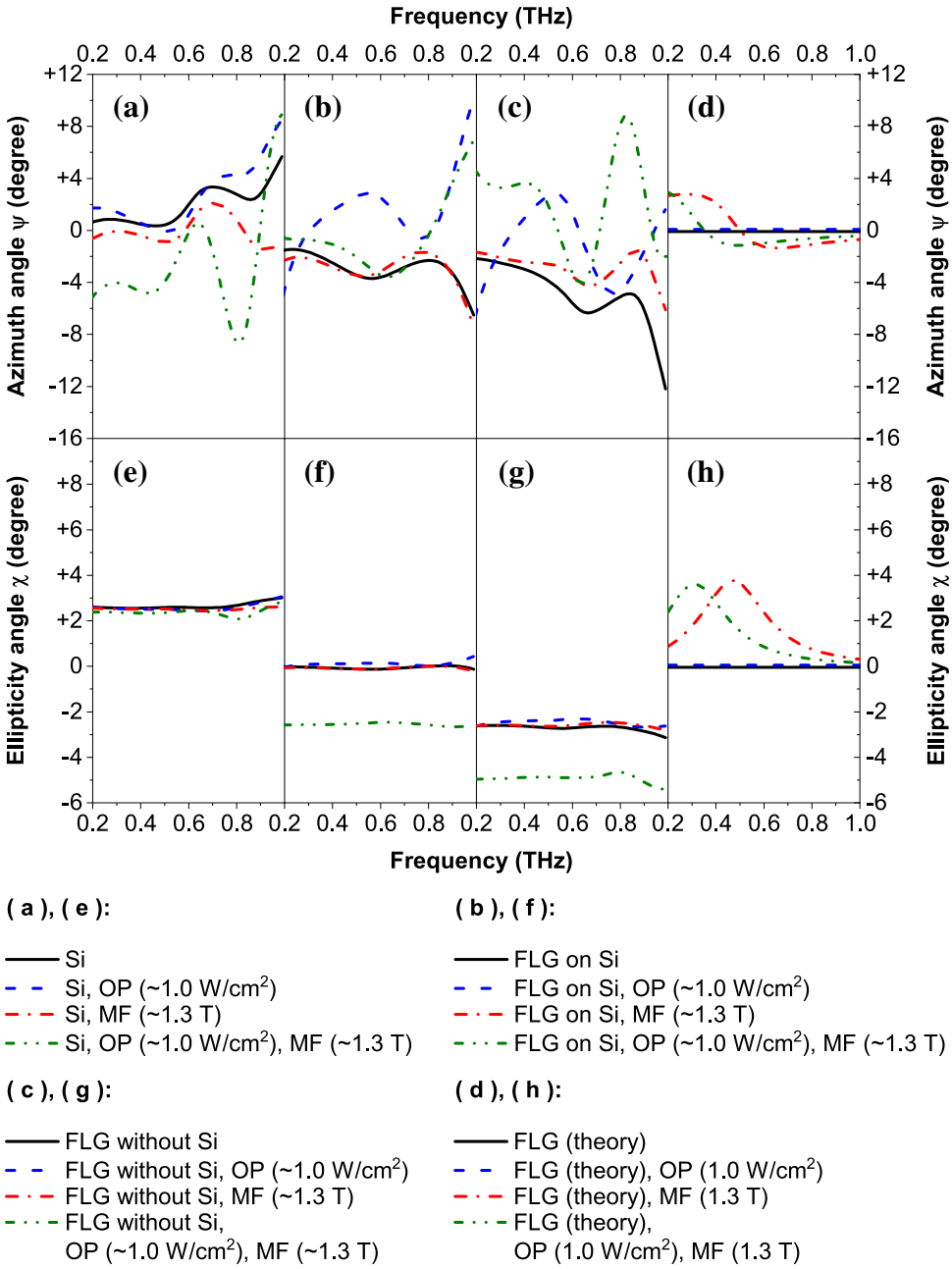

Fig. 7 Frequency dependencies of the azimuth angle ψ of the polarization ellipse of the electromagnetic waves transmitted through **a** the Si substrate (experimental data), **b** the FLG on the Si substrate (experimental data), **c** the FLG without the Si substrate (experimental data), and **d** the FLG without the Si substrate (theoretical data); and frequency dependencies of the ellipticity angle χ of the polarization ellipse of the electromagnetic waves transmitted through **e** the Si substrate (experimental data), **f** the FLG on the Si substrate (experimental data), **g** the FLG without the Si substrate (experimental data), and **h** the FLG without the Si substrate (theoretical data) under the various external influences

5 Conclusion

As a result of this work, the polarization properties of the FLG on the Si substrate in the THz frequency range were studied. It can be seen that the FLG is an efficient material for creation of the magneto-optically tunable polarization modulators, which are necessary in cutting-edge THz nanophotonics.

The next stage of this work is a theoretical and an experimental study of the polarization properties of graphene at different values of the external OP and the external static MF.

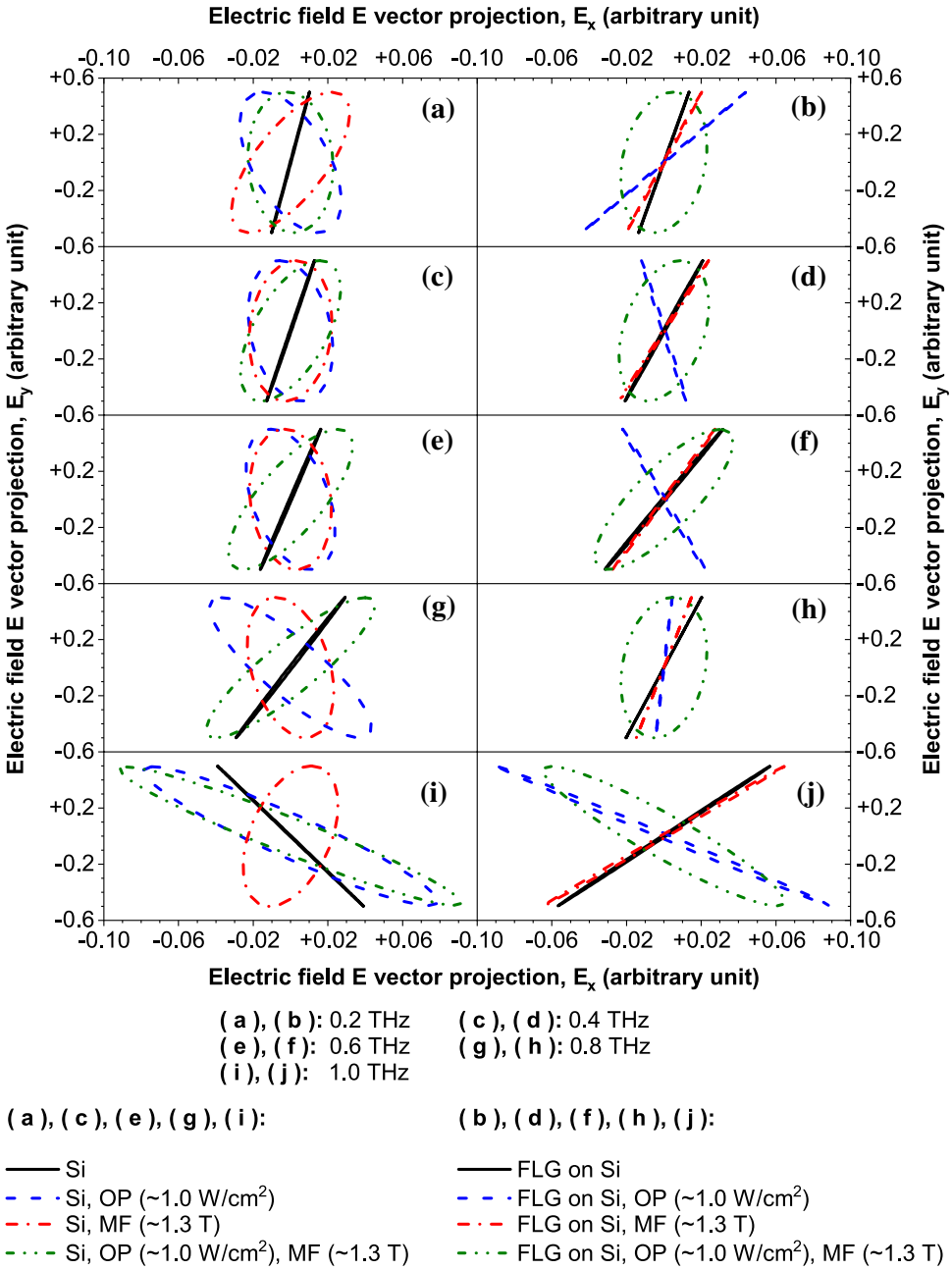

Fig. 8 Polarization ellipse of the electromagnetic waves at the frequency of 0.2 THz transmitted through **a** the Si substrate, and **b** the FLG on the Si substrate; at the frequency of 0.4 THz transmitted through **c** the Si substrate, and **d** the FLG on the Si substrate; at the frequency of 0.6 THz transmitted through **e** the Si substrate, and **f** the FLG on the Si substrate; at the frequency of 0.8 THz transmitted through **g** the Si substrate, and **h** the FLG on the Si substrate; at the frequency of 1.0 THz transmitted through **i** the Si substrate, and **j** the FLG on the Si substrate under the various external influences

Acknowledgements The authors are very grateful to professor A. V. Baranov, Sc.D., and K. V. Bogdanov, Ph.D., researchers at ITMO University's Centre of Information Optical Technology (Russian Federation), for the characterization of the FLG using the SEM and the Raman spectroscopy systems. The reported study was funded by the Government of the Russian Federation, Grant Number 08–08 (Project 5–100).

Compliance with ethical standards

Conflict of interest On behalf of all authors, the corresponding author states that there is no conflict of interest.

References

1. Hafez HA, Chai X, Ibrahim A, Mondal S, Férachou D, Ropagnol X, Ozaki T (2016) Intense terahertz radiation and their applications. J Opt 18(9):093004. https://doi.org/10.1088/2040-8978/18/9/093004
2. Consolino L, Bartalini S, De Natale P (2017) Terahertz frequency metrology for spectroscopic applications: a review. J Infrared Millim Terahertz Waves 38(11):1289–1315. https://doi.org/10.1007/s10762-017-0406-x
3. Smirnov S, Anoshkin IV, Demchenko P, Gomon D, Lioubtchenko DV, Khodzitsky M, Oberhammer J (2018) Optically controlled dielectric properties of single-walled carbon nanotubes for

terahertz wave applications. Nanoscale 10(26):12291–6. https://doi.org/10.1039/C8NR03740J
4. Yin M, Tang S, Tong M (2016) The application of terahertz spectroscopy to liquid petrochemicals detection: a review. Appl Spectrosc Rev 51(5):379–396. https://doi.org/10.1080/05704928.2016.1141291
5. Yang X, Zhao X, Yang K, Liu Y, Liu Y, Fu W, Luo Y (2016) Biomedical applications of terahertz spectroscopy and imaging. Trends Biotechnol 34(10):810–824. https://doi.org/10.1016/j.tibtech.2016.04.008
6. Soboleva VY, Gusev SI, Khodzitsky MK (2018) Metafilm-based biosensor for determination of glucose concentration in human blood. Sci Technol J Inf Technol Mech Opt 18(3):377–83. https://doi.org/10.17586/2226-1494-2018-18-3-377-383
7. Guerboukha H, Nallappan K, Skorobogatiy M (2018) Toward real-time terahertz imaging. Adv Opt Photonics 10(4):843–938. https://doi.org/10.1364/AOP.10.000843
8. Litvinov EA, Vozianova AV, Khodzitsky MK (2018) Epsilon-near-zero metal-dielectric composite for terahertz frequency range. J Phys Conf Ser 1062:012010. https://doi.org/10.1088/1742-6596/1062/1/012010
9. Masyukov MS, Vozianova AV, Grebenchukov AN, Khodzitsky MK (2018) Graphene-based tunability of chiral metasurface in terahertz frequency range. J Phys Conf Ser 1124:051053. https://doi.org/10.1088/1742-6596/1124/5/051053
10. Dhillon SS et al (2017) The 2017 terahertz science and technology roadmap. J Phys D Appl Phys 50(4):043001. https://doi.org/10.1088/1361-6463/50/4/043001
11. Mittleman DM (2017) Perspective: terahertz science and technology. J Appl Phys 122(23):230901. https://doi.org/10.1063/1.5007683
12. Hashemi MR, Cakmakyapan S, Jarrahi M (2017) Reconfigurable metamaterials for terahertz wave manipulation. Rep Prog Phys 80(9):094501. https://doi.org/10.1088/1361-6633/aa77cb
13. DegI'Innocenti R, Kindness SJ, Beere HE, Ritchie DA (2017) All-integrated terahertz modulators. Nanophotonics 7(1):127–144. https://doi.org/10.1515/nanoph-2017-0040
14. Shi J, Li Z, Sang DK, Xiang Y, Li J, Zhang S, Zhang H (2018) THz photonics in two dimensional materials and metamaterials: properties, devices and prospects. J Mater Chem C Mater 6(6):1291–1306. https://doi.org/10.1039/c7tc05460b
15. Cheng J, Fan F, Chang S (2019) Recent progress on graphene-functionalized metasurfaces for tunable phase and polarization control. Nanomaterials. https://doi.org/10.3390/nano9030398
16. Gu XQ, Yin WY (2014) Terahertz wave responses of dispersive few-layer graphene (FLG) and ferroelectric film composite. Opt Commun 319:70–74. https://doi.org/10.1016/j.optcom.2014.01.012
17. Ryzhii V, Ryzhii M, Mitin V, Shur MS, Otsuji T (2015) Negative terahertz conductivity in remotely doped graphene bilayer heterostructures. J Appl Phys 118(18):183105. https://doi.org/10.1063/1.4934856
18. Fu M, Quan B, He J, Yao Z, Gu C, Li J, Zhang Y (2016) Ultrafast terahertz response in photoexcited, vertically grown few-layer graphene. Appl Phys Lett 108(12):121904. https://doi.org/10.1063/1.4944887
19. Fu M, Wang X, Ye J, Feng S, Sun W, Han P, Zhang Y (2018) Strong negative terahertz photoconductivity in photoexcited graphene. Opt Commun 406:234–238. https://doi.org/10.1016/j.optcom.2017.01.045
20. Tomadin A et al (2018) The ultrafast dynamics and conductivity of photoexcited graphene at different Fermi energies. Sci Adv. https://doi.org/10.1126/sciadv.aar5313
21. Heyman JN, Foo Kune RF, Alebachew BA, Nguyen MD, Robinson JT (2014) Ultrafast terahertz Faraday rotation in graphene. J Appl Phys 116(21):214302. https://doi.org/10.1063/1.4903212
22. Qin J et al (2018) Enhanced Faraday rotation and magneto-optical figure of merit in gold grating/graphene/silicon hybrid magneto-plasmonic devices. APL Photonics 3(1):016103. https://doi.org/10.1063/1.5008775
23. Liu JQ, Wu S, Zhou YX, He MD, Zayats AV (2018) Giant Faraday rotation in graphene metamolecules due to plasmonic coupling. J Lightw Technol 36(13):2606–2610. https://doi.org/10.1109/JLT.2018.2818712
24. Mei H, Xu W, Wang C, Yuan H, Zhang C, Ding L, Zhang J, Deng C, Wang Y, Peeters FM (2018) Terahertz magneto-optical properties of bi- and tri-layer graphene. J Phys Condens Matter 30(17):175701. https://doi.org/10.1088/1361-648X/aab81d
25. Grebenchukov AN, Azbite SE, Zaitsev AD, Khodzitsky MK (2019) Faraday effect control in graphene-dielectric structure by optical pumping. J Magn Magn Mater 472:25–28. https://doi.org/10.1016/j.jmmm.2018.09.110
26. Aschaffenburg DJ, Williams MRC, Schmuttenmaer CA (2016) Terahertz spectroscopic polarimetry of generalized anisotropic media composed of archimedean spiral arrays: experiments and simulations. J Chem Phys 144(17):174705. https://doi.org/10.1063/1.4947469
27. Wu L, Salehi M, Koirala N, Moon J, Oh S, Armitage NP (2016) Quantized Faraday and Kerr rotation and axion electrodynamics of a 3D topological insulator. Science 354(6316):1124–1127. https://doi.org/10.1126/science.aaf5541
28. Mosley CDW, Failla M, Prabhakaran D, Lloyd-Hughes J (2016) Terahertz spectroscopy of anisotropic materials using beams with rotatable polarization. Sci Rep. https://doi.org/10.1038/s41598-017-12568-0
29. Sanjuan F, Gaborit G, Coutaz JL (2018) Full electro-optic terahertz time-domain spectrometer for polarimetric studies. Appl Opt 57(21):6055–6060. https://doi.org/10.1364/AO.57.006055
30. Zhao G, Savini G, Yu Y, Li S, Zhang J, Ade P (2019) A dual-port THz time domain spectroscopy system optimized for recovery of a sample's Jones matrix. Sci Rep. https://doi.org/10.1038/s41598-019-39322-y
31. Kovalska E, Lesongeur P, Hogan BT, Baldycheva A (2019) Multilayer graphene as a selective detector for future lung cancer biosensing platforms. Nanoscale 11(5):2476–2483. https://doi.org/10.1039/C8NR08405J
32. Bogdanov K, Fedorov A, Osipov V, Enoki T, Takai K, Hayashi T, Ermakov V, Moshkalev S, Baranov A (2014) Annealing-induced structural changes of carbon onions: high-resolution transmission electron microscopy and Raman studies. Carbon 73:78–86. https://doi.org/10.1016/j.carbon.2014.02.041
33. Wu JB, Lin ML, Cong X, Liu HN, Tan PH (2018) Raman spectroscopy of graphene-based materials and its applications in related devices. Chem Soc Rev 47(5):1822–1873. https://doi.org/10.1039/C6CS00915H
34. Bespalov VG, Gorodetskiĭ AA, Denisyuk IY, Kozlov SA, Krylov VN, Lukomskiĭ GV, Petrov NV, Putilin SE (2008) Methods of generating superbroadband terahertz pulses with femtosecond lasers. J Opt Technol 75(10):636–642. https://doi.org/10.1364/JOT.75.000636

35. Ferguson B, Abbott D (2001) De-noising techniques for terahertz responses of biological samples. Microelectron J 32(12):943–953. https://doi.org/10.1016/S0026-2692(01)00093-3
36. Born M, Wolf E (2005) Principles of optics: electromagnetic theory of propagation, interference and diffraction of light, 7th (expanded) edn. Cambridge University Press, Cambridge
37. Shuvaev A, Pimenov A, Astakhov GV, Mühlbauer M, Brüne C, Buhmann H, Molenkamp LW (2013) Room temperature electrically tunable terahertz Faraday effect. Appl Phys Lett 102(24):241902. https://doi.org/10.1063/1.4811496